Journal of Power Sources 217 (2012) 114–119

Contents lists available at SciVerse ScienceDirect

Journal of Power Sources

journal homepage: www.elsevier.com/locate/jpowsour

A novel ceria-based solid oxide fuel cell free from internal short circuit

Wenping Sun [a,b], Wei Liu [a,c,*]

[a] CAS Key Laboratory of Materials for Energy Conversion, Department of Materials Science and Engineering, University of Science and Technology of China (USTC), Hefei 230026, PR China
[b] School of Materials Science and Engineering, Georgia Institute of Technology, 771 Ferst Drive, Atlanta, Georgia, 30332-0245, USA
[c] Key Laboratory of Materials Physics, Institute of Solid State Physics, Chinese Academy of Sciences, Hefei 230031, PR China

HIGHLIGHTS

- A novel ceria-based solid oxide fuel cell (SOFC) was designed employing barium-containing anode.
- A thin electron-blocking layer was formed in situ at the anode/electrolyte interface.
- The electron-blocking layer eliminated the internal short circuit of ceria-based SOFC effectively.
- The new cell can output excellent power performances at low temperatures at high efficiency.

GRAPHICAL ABSTRACT

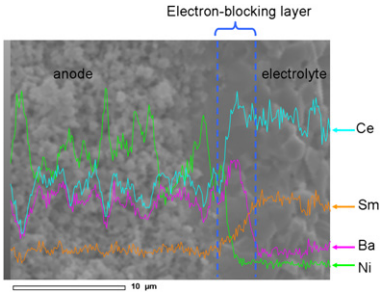

ARTICLE INFO

Article history:
Received 30 March 2012
Received in revised form
22 May 2012
Accepted 23 May 2012
Available online 6 June 2012

Keywords:
Ceria
Internal short circuit
Open circuit voltage
Solid oxide fuel cell

ABSTRACT

A novel solid oxide fuel cell (SOFC) is designed and investigated in this work. Barium-containing anode is employed for $Ce_{0.8}Sm_{0.2}O_{2-\delta}$ (SDC)-based SOFC. SEM and EDX results show that barium diffuses from the anode to the electrolyte and a thin $BaO–CeO_2–Sm_2O_3$ ternary composite interlayer is formed in situ at elevated temperatures. The interlayer is electron-blocking, and eliminates the well-known internal short circuit in the SDC electrolyte membrane completely. Consequently, the open circuit voltages (OCVs) of the cell are improved significantly and achieve as high as 1.04, 1.06, 1.07, and 1.08 V at 700, 650, 600, and 550 °C, respectively, for the cell co-fired at 1350 °C. Notably, the new cell still outputs 221 mW cm^{-2} at a voltage of 0.9 V at 600 °C, while the traditional ceria-based cell cannot output any performance at all at such a high voltage. The results demonstrate that this novel structured cell exhibits great potential working at low temperatures at high efficiency.

1. Introduction

Solid oxide fuel cell (SOFC) is the most efficient electrochemical device for converting chemical energy directly into electrical energy. However, the widespread commercial application of SOFC still has a long way to go, which is mainly caused by the high operating temperature. High operating temperature not only limits materials selection but also results in high fabrication cost and performance degradation rate. Hence, reducing the operating temperature to intermediate or lower temperatures is the top priority for SOFC nowadays [1–5]. The decrease of operating temperature demands an electrolyte with high ionic conductivity at reduced temperatures. Compared with the conventional oxide ionic conductor yttria-stabilized zirconia (YSZ), rare earth-doped ceria exhibits sufficiently high oxide ionic conductivity and is considered to be a very promising alternative electrolyte material for intermediate/low-temperature SOFC [1,3,5,6]. Therefore, SOFC based on doped ceria electrolyte has been attracting more and more attention in the past two decades. However, Ce^{4+} in ceria can

* Corresponding author. CAS Key Laboratory of Materials for Energy Conversion, Department of Materials Science and Engineering, University of Science and Technology of China (USTC), Hefei 230026, PR China. Tel.: +86 0551 3606929; fax: +86 0551 3602586.
E-mail address: wliu@ustc.edu.cn (W. Liu).

0378-7753/$ – see front matter © 2012 Elsevier B.V. All rights reserved.
http://dx.doi.org/10.1016/j.jpowsour.2012.05.065

be easily reduced to Ce^{3+} in reduced atmospheres at elevated temperatures [7–9]. The reduction behavior would not only lead to mechanical degradation of the electrolyte due to the crystal lattice expansion but also induce n-type electronic conduction through the electrolyte. The n-type conduction behavior induces partial internal short circuit, and then results in remarkable decrease of open circuit voltages (OCVs) of a fuel cell [10,11]. Low OCVs mean low energy efficiency for the cell and lead to obvious energy losses, which is undesirable in practical applications [5].

To overcome the problems caused by the inherent drawbacks of doped ceria, various strategies were developed. Depositing a thin YSZ film on the doped ceria electrolyte membrane via sputtering or sol–gel coating process was widely employed to block electronic conduction [7,12–14]. After introducing a 3-μm-thick YSZ thin film, the OCV of the cell with gadolinium-doped ceria electrolyte increased from 0.59 V to 1.05 V at 800 °C [13]. However, it must be noted that the YSZ layer will increase ohmic resistance of the cell due to the lower ionic conductivity of YSZ at low/intermediate temperatures. Therefore, it is necessary to investigate highly conductive alternatives as electron-blocking layer for cells based on doped ceria. Wachsman et al. proposed a graded ceria/bismuth oxide bi-layered electrolyte, where highly conductive bismuth oxide acted as the electronic barrier, and fabricated very high performance cells with improved OCVs [5,15–19]. However, bismuth oxide also seems not to be a very desirable choice because partial internal short circuit really exists in such a bi-layered electrolyte judging by OCVs of the cells, which are still lower than 1 V at 650 °C. At the same time, Takashi Hibino and co-workers introduced a thin doped-$BaCeO_3$ layer, which is a good mixed ionic conductor, to block the internal short circuit and also obtained exciting results. In their early work, they fabricated $Ce_{0.8}Sm_{0.2}O_{2-\delta}$/$BaCe_{1-x}Sm_xO_{3-\delta}$ bi-layered electrolyte by coating BaO slurry on $Ce_{0.8}Sm_{0.2}O_{1.9}$ (SDC) pellet followed by a solid state reaction between SDC and BaO [20], and they also prepared $Ce_{0.9}Gd_{0.1}O_{1.95}$/$BaCe_{1-x}Gd_xO_{3-\delta}$/$Ce_{0.9}Gd_{0.1}O_{1.95}$ multilayered electrolyte via a similar technique [21]. Subsequently, they tried to fabricate multilayered $Ce_{0.9}Gd_{0.1}O_{1.95}$/$BaCe_{0.8}Y_{0.2}O_{3-\delta}$/$Ce_{0.9}Gd_{0.1}O_{1.95}$ electrolyte by the tape-casting process on the Ni–SDC anode support, using $BaCe_{0.8}Y_{0.2}O_{3-\delta}$ as the raw material in stead [22]. The results demonstrated that both methods could suppress the electronic current through the electrolyte membrane effectively.

Here, we propose a new and facile strategy that a barium-containing anode, Ni–$BaZr_{0.1}Ce_{0.7}Y_{0.2}O_{3-\delta}$ (Ni–BZCY) cermet, is directly employed for SDC-based SOFC. In this case, a considerable amount of barium in the anode will diffuse to the SDC electrolyte membrane and then react with SDC forming a thin BaO–CeO_2–Sm_2O_3 ternary composite interlayer in situ. It is expected that internal short circuit in the cell will be suppressed, and correspondingly improved OCV values can be attained.

2. Experimental

2.1. Synthesis of powders

$Ce_{0.8}Sm_{0.2}O_{2-\delta}$ (SDC) powders used for the electrolyte, NiO–BZCY composite powders for anode functional layer and BZCY powders for the anode substrate were all synthesized via a citric acid–nitrate gel combustion process [23]. The as-prepared SDC powders were calcined at 700 °C for 3 h in air, while NiO–BZCY and BZCY powders were calcined at 1000 °C for 3 h in air.

2.2. Fabrication of fuel cells

The NiO–BZCY powders for anode substrate were prepared by mixing BZCY, NiO and starch in a weight ratio of 40:60:20 mechanically, and starch worked as the pore-creating material. NiO–BZCY composite powders synthesized via the combustion process were used for preparing anode functional layer. The anode-supported half cells were fabricated by a dry-pressing method [24]. First, the NiO–BZCY powders were pressed in a stainless steel module to form an anode substrate with a flat surface and a certain mechanical strength. Then, the loose NiO–BZCY composite powders were distributed onto the substrate and pressed again. Subsequently, SDC powders were added and evenly distributed onto the substrate. The SDC powder layer was then pressed together with the anode, obtaining the green half cell. The thickness of the SDC membrane could be controlled by varying the amount of SDC powders. Finally, the green half cells were co-fired at 1100, 1150, 1200, 1250, 1300 or 1350 °C for 5 h. For comparison, typical SDC-based half cells were also fabricated via the same dry-pressing method. SDC, NiO and starch mixed in a weight ratio of 40:60:20 were used as anode powders. The half cells were co-fired at 1400 °C for 5 h to get a dense SDC electrolyte membrane. $Sm_{0.5}Sr_{0.5}CoO_{3-\delta}$–$Ce_{0.8}Sm_{0.2}O_{2-\delta}$ (SSC–SDC) composite slurry was brush-painted on the electrolyte membrane and then sintered at 950 °C for 3 h in air to form a porous cathode layer.

2.3. Electrochemical measurement and other characterizations

Single cells were tested in a home-made cell testing system with humidified hydrogen (2% H_2O) as the fuel and the static air as the oxidant, respectively. The flow rate of fuel gas was about 40 ml min^{-1}. Ag paste was applied to the cathode as a current collector and Ag wire was employed as the conducting wire. *I–V* curves of the cells were collected with a DC Electronic Load (ITech Electronics model IT8511) based on the two-probe configuration. The electrochemical impedance spectra (EIS) of the cells were measured under open circuit conditions using an impedance analyzer (CHI604B, Shanghai Chenhua). A 5 mV a.c. signal was applied and the frequency was swept from 100 kHz to 0.1 Hz. The spectrum curve fitting was performed using the ZSimpWin Software. Phase structure was identified by an X-ray diffractometer (Rigaku TTR-III) using CuKα radiation. A scanning electron microscopy (SEM, JEOL JSM-6700F) equipped with an energy-dispersive X-ray spectroscopy (EDS) system was used to perform the microstructure and chemical analysis.

3. Results and discussion

Fig. 1 shows the SEM–EDS analysis in line-scan mode at the anode/electrolyte interface of a cell co-fired at 1350 °C for 5 h.

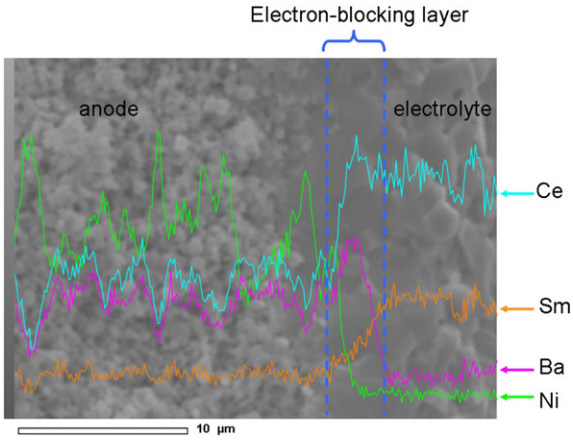

Fig. 1. SEM–EDS analysis in line-scan mode at the anode/electrolyte interface of the cell co-fired at 1350 °C for 5 h.

Obviously, an interlayer containing Ba, Ce, Sm, and a slight bit of Ni can be observed at the anode/electrolyte interface, indicating that the element diffusion of Ba and Ni from the anode to the SDC electrolyte membrane occurred. Given Zr and Y only occupy very few portions in the anode, the diffusion behavior of Zr and Y was ignored here. It can be found that Ni only existed in the area very near to the anode, which will not contribute electronic conduction through the electrolyte membrane. Notably, the content of Ba and Ni decreased gradually with the distance getting far away from the anode. The diffusion behavior was also confirmed by the result of the SEM–EDS analysis in area-scan mode (Fig. S1). According to the element distribution, it can be concluded that a thin $BaO–CeO_2–Sm_2O_3$ ternary composite interlayer was formed just at the anode/electrolyte interface. Moreover, the XRD pattern of the electrolyte membrane surface (Fig. 2) showed that only peaks corresponding to fluorite-structured $Ce_{0.8}Sm_{0.2}O_{2-\delta}$ (SDC) could be found, indicating that the electrolyte was exactly a bi-layered membrane.

Fig. 3 shows the OCVs of the cell co-fired at 1350 °C, as compared with the theoretical Nernst voltages and OCVs of those typical doped ceria-based cells. Owing to the well-known internal short circuit, the OCVs of the doped CeO_2-based cells generally range from 0.89 to 0.75 V at temperatures between 550 and 700 °C. Surprisingly, the OCVs substantially increased after introducing the $BaO–CeO_2–Sm_2O_3$ interlayer, and achieved as high as 1.04, 1.06, 1.07, and 1.08 V at 700, 650, 600, and 550 °C, respectively. The OCVs were already very close to the theoretical Nernst voltages, especially compared with the values of those traditional ceria-based cells, revealing that the interlayer definitely blocked the electronic current through the electrolyte membrane effectively. Most importantly, the improved OCVs ensure that the cell can work at much higher voltage efficiency and ultimately total efficiency now. As reported, $BaO–CeO_2–Ln_2O_3$ (Ln = Sm and Gd) ternary system actually consists of two phases of acceptor-doped $BaCeO_3$ and CeO_2, and $BaCeO_3$-based ionic conductor can effectively block electron transport. Thus, the OCVs of the fuel cell increased significantly when the $BaCeO_3–CeO_2$ based composite conductors were used as electrolyte in stead of doped-CeO_2 [31,32]. For example, the OCV value achieved 0.976 V for $BaCe_{0.8}Sm_{0.2}O_{3-\delta}–Ce_{0.8}Sm_{0.2}O_{2-\delta}$ (BCS–SDC, weight ratio 1:1) electrolyte and 0.95 V for $BaCe_{0.8}Gd_{0.2}O_{3-\delta}–Ce_{0.8}Gd_{0.2}O_{2-\delta}$ (BCG–GDC, molar ratio 2:3). Similarly, the incorporated $BaO–CeO_2–Sm_2O_3$ interlayer should be responsible for the OCV improvement of the new cell. For the contribution to block electron transport, the $BaO–CeO_2–Sm_2O_3$ interlayer is referred to as an electron-blocking layer.

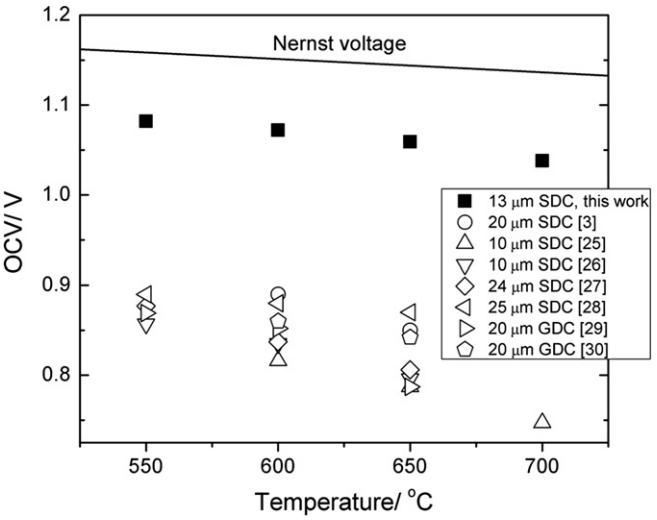

Fig. 3. OCVs of the novel cell co-fired at 1350 °C for 5 h, as compared with the theoretical Nernst voltages and OCVs of those typical doped ceria-based fuel cells reported in literatures.

Notably, considerable diffusion behavior of Ba still occurred when the cell was co-fired at a low temperature of 1100 °C, and correspondingly the electro-blocking layer was also formed. As is well-known, element diffusion rate is highly dependent on the temperature, and hence the thickness of the electron-blocking layer should be closely related with the co-firing temperature. Fig. 4 shows the estimated thickness of the electron-blocking layer formed at various co-firing temperatures. The thickness of the electron-blocking layer got thinner with the co-firing temperature, and ranged from about 3 to 0.7 μm with decreasing the co-firing temperature from 1350 to 1100 °C for 5 h. Meanwhile, the electrolyte membrane density was also highly dependent on the co-firing temperature. The SEM images of the surface morphologies of the electrolyte membranes sintered at different temperatures are shown in Fig. 5. As can be seen, the membrane didn't get dense till co-fired at temperatures higher than 1200 °C. Also, the grain size in the membrane gradually grew larger and larger as increasing the co-firing temperature. As expected, the OCVs of the cells with dense electrolyte membranes were all higher than 1.02 V at 700 °C, as shown in Fig. 6, and the results further evidenced that the

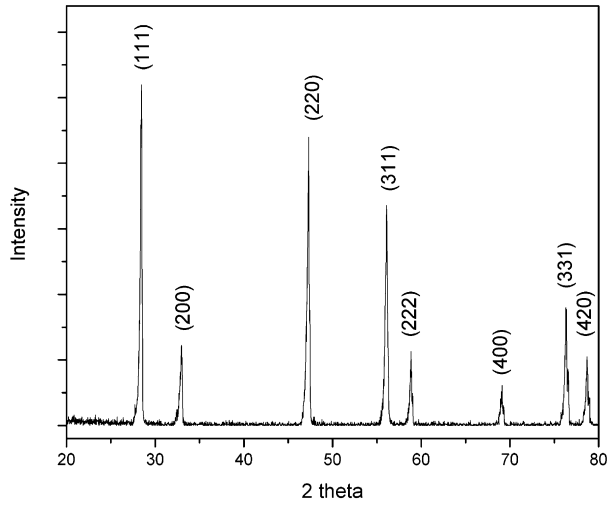

Fig. 2. XRD pattern of the surface of the as-prepared electrolyte membrane co-fired at 1350 °C for 5 h.

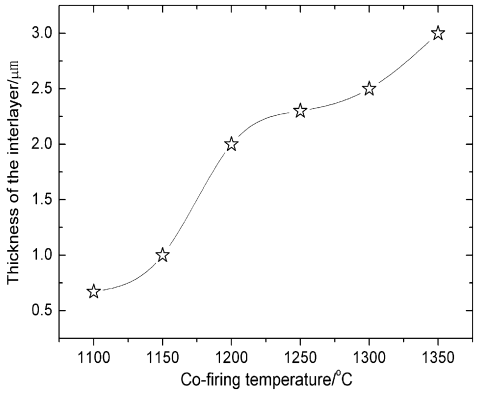

Fig. 4. Estimated thickness of the electron-blocking layer formed at different co-firing temperatures.

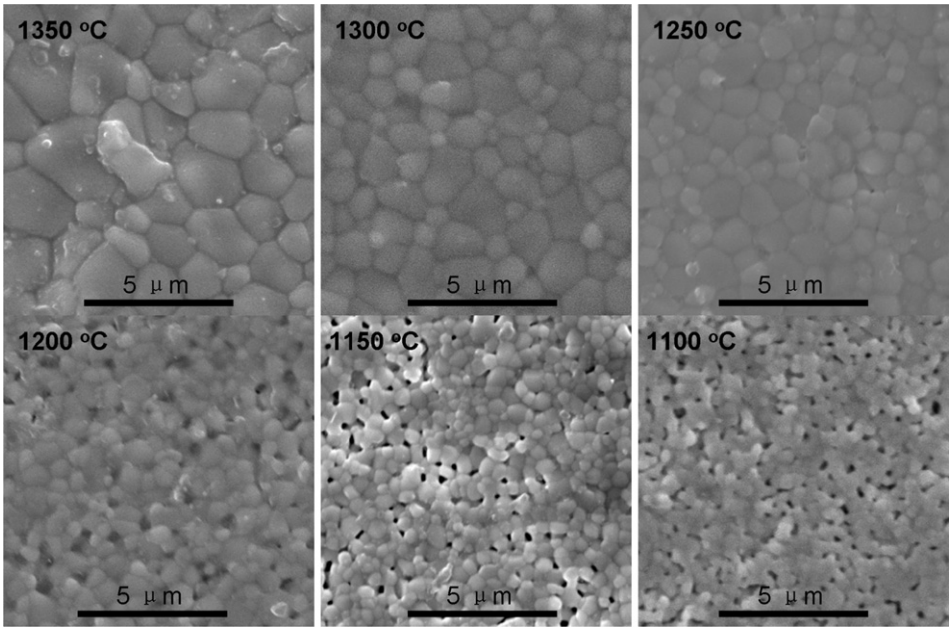

Fig. 5. SEM images of the surface morphologies of the electrolyte membranes co-fired at different temperatures.

interlayer was electron-blocking. Moreover, the OCVs of the cell co-fired at 1150 °C still achieved as high as 0.93, 0.97, 1.03, and 1.04 V at 700, 650, 600, and 550 °C, respectively. However, as can be seen from Fig. 7, the electrolyte membrane of the cell co-fired at 1150 °C was not dense at all except for the electron-blocking interlayer. Given the relatively high OCVs of the cell, we can conclude that the electron-blocking interlayer formed at 1150 °C was already quite dense to block gas leakage. Besides, Fig. 7 also exhibits another typical demonstration of the electron-blocking interlayer formed in this novel structured cell.

To evaluate the cell performance after introducing an electron-blocking layer, a single cell co-fired at 1350 °C using SSC–SDC as cathode was tested with humidified hydrogen (2% H_2O) as the fuel and ambient air as the oxidant, and the cell is hereafter referred to as "Cell-improved". Fig. 8 shows a typical SEM image of the cross section of the tested cell. The electrolyte membrane was about 13 μm in thickness and fully dense without any pores. Moreover, the electrodes bonded firmly to the electrolyte membrane, suggesting good compatibility between the electrodes and the electrolyte membrane. Fig. 9(a) shows the *I–V* and power density curves of Cell-improved. The maximum power densities achieved 1006, 752, and 511 mW cm^{-2} at 700, 650, and 600 °C, respectively. In contrast, the maximum power densities of a typical SDC-based cell (the cell is hereafter referred to as "Cell-unimproved", Fig. S2) fabricated via the same process as Cell-improved were only 480 and 364 mW cm^{-2} at 650 and 600 °C, respectively, as shown in Fig. 9(b). Shown in Fig. 9(c) are the power densities measured at different output voltages for the two cells at 600 °C. Clearly, the

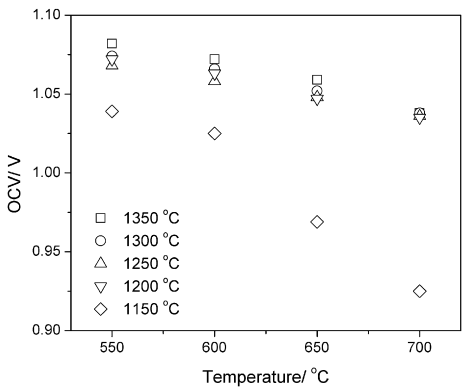

Fig. 6. OCVs of the cells co-fired at different temperatures for 5 h.

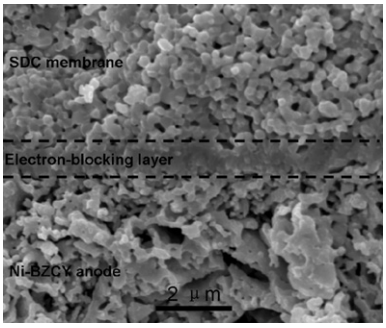

Fig. 7. The SEM image of the cross section of the cell co-fired at 1150 °C for 5 h.

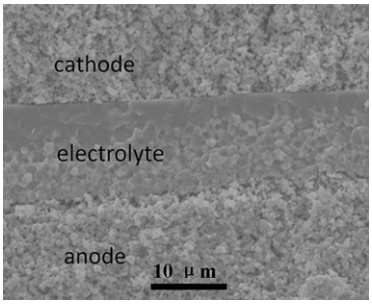

Fig. 8. A typical SEM image of the cross section of the tested Cell-improved.

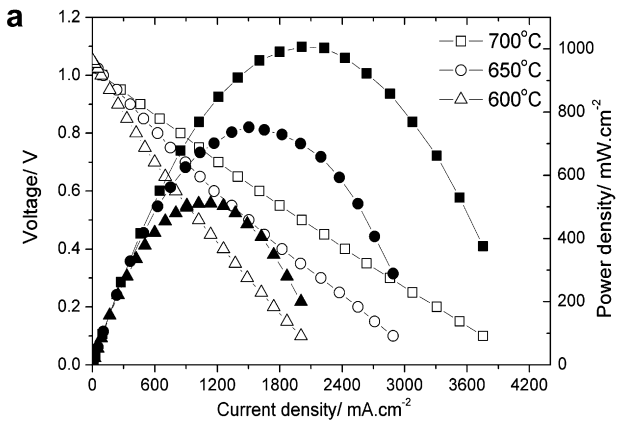

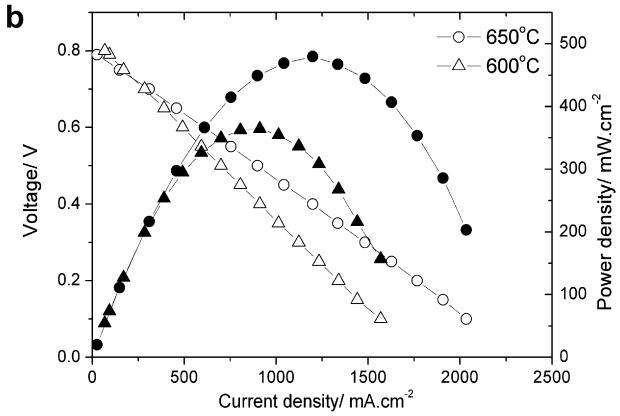

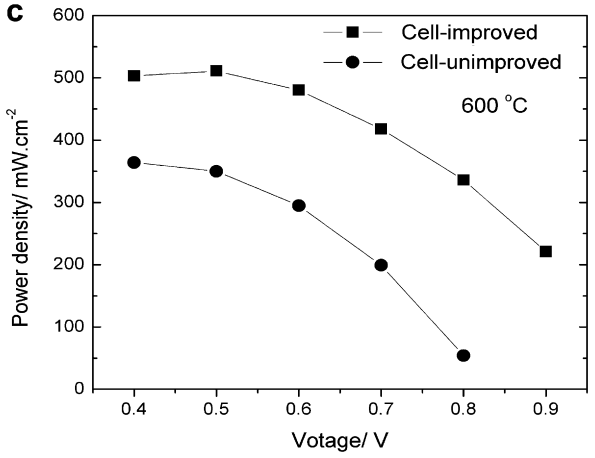

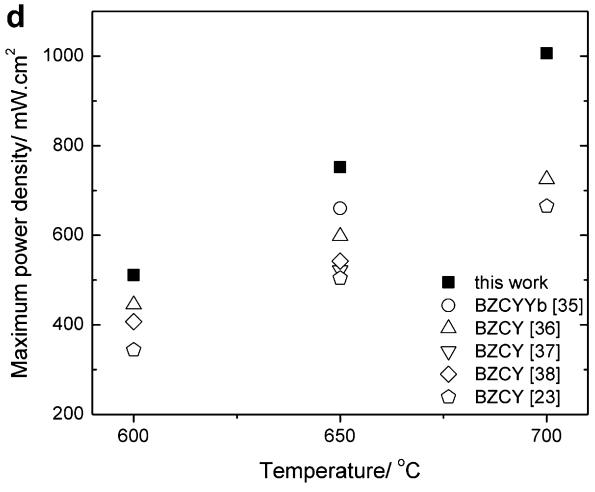

performance superiority of Cell-improved gets more and more significant with increasing the output voltage to attain a high working efficiency. The significant improvement of the cell performances should be definitely attributed to the highly improved OCV values of Cell-improved. Actually, the maximum power densities of Cell-improved were lower than those best values reported in literatures for ceria-based fuel cells [3,30], and this might be induced by different electrode materials and fabrication process of fuel cells. However, Cell-improved exhibited an unsurpassed advantage that it could work at high output voltages, which is highly desired in practical devices. Excitingly, Cell-improved still output 221 mW cm^{-2} at a cell voltage of 0.9 V at 600 °C, while Cell-unimproved and other ceria-based cells in literatures could not output any performance at all at such a high output voltage [3,25–30]. Moreover, the performance of Cell-improved is even more superior to the best reported performances by far of the state-of-the-art proton-conducting SOFC based on acceptor-doped barium cerate, such as BZCY and $BaZr_{0.1}Ce_{0.7}Y_{0.1}Yb_{0.1}O_{3-\delta}$ (BZCYYb), which is widely considered to be the most promising low-temperature SOFC [23,33–38], as shown in Fig. 9(d). The results demonstrate that Cell-improved is indeed a potential alternative fuel cell working at high efficiency while outputting excellent power densities at low temperatures.

Interestingly, the electron-blocking layer also affected the polarization resistances of the cell a lot. Fig. 10 shows typical electrochemical impedance spectra (EIS) of the two cells measured at 650 and 600 °C under open circuit conditions. The intercept with the real axis at high frequencies represents the ohmic resistance (R_{ohm}) of the cell, which is mainly contributed by the electrolyte resistance; the difference between the high frequency and the low frequency intercepts with the real axis represents the polarization resistance (R_p) of the cell, which is mainly determined by the microstructure of the electrodes and the electrode/electrolyte interfaces. As can be seen from Fig. 10, the polarization behavior was influenced greatly when the electron-blocking composite was introduced to the anode/electrolyte interface. The polarization resistances of Cell-improved were unexpectedly over two times larger than those of the Unimproved-cell. The R_p values of Cell-unimproved were only 0.05 and 0.15 Ω cm^2 at 650 and 600 °C, respectively, while the values increased to 0.21 and 0.46 Ω cm^2 for Cell-improved. As reported previously [39,40], the internal short circuit current of the electrolyte could accelerate the electrode reaction including the charge transfer on the surface and the oxygen-ion diffusion into the electrolyte, and then leads to the reduction of the polarization resistance. Hence, the increased R_p values of Cell-improved should be caused by the elimination of the internal short circuit current through the electrolyte membrane. On the other hand, the ohmic resistances of Cell-improved were lower than those of Cell-unimproved, and this should be attributed to the higher electrolyte membrane density of Cell-improved, which is fully dense without any pores, while obvious pores can be observed in the SDC membrane of Cell-unimproved (Fig. S2). Besides, the excellent anode/electrolyte interface microstructure should also contribute to the lower ohmic resistances of Cell-improved (Fig. 8). Although the total resistance (the sum of R_p and R_{ohm}) of Cell-improved was somewhat high, the significantly improved high OCV ensured the excellent power performance of the cell.

Fig. 9. (a) *I–V* and power density curves of the Cell-improved with electrolyte co-fired at 1350 °C for 5. (b) *I–V* and power density curves of the Cell-unimproved with SDC electrolyte co-fired at 1400 °C for 5. (c) Power densities measured at different output voltages for the two cells at 600 °C. (d) The maximum power densities of Cell-improved, as compared with those of the state-of-the-art proton-conducting SOFC.

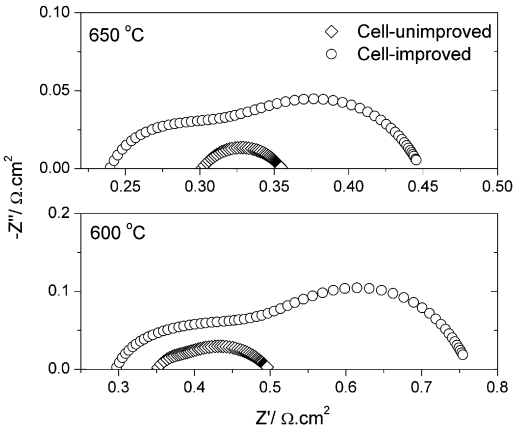

Fig. 10. Electrochemical impedance spectra (EIS) of Cell-improved and Cell-unimproved measured at 650 and 600 °C under open circuit conditions.

4. Conclusions

In summary, an electron-blocking layer was successfully incorporated via in situ reaction at the anode/electrolyte interface when the barium-containing Ni–BZCY cermet was employed as anode for SDC-based SOFC. The thickness of the electron-blocking layer was dependent on the co-firing temperature. The OCVs of the new engineered cell were greatly improved, indicating that the electron-blocking layer could eliminate internal short circuit in SDC membrane effectively. The new cell turns out to be a very promising high efficiency fuel cell working at low temperatures for practical applications. Importantly, this novel design strategy makes doped ceria ionic conductors become really competitive electrolytes for low/intermediate-temperature SOFC.

Acknowledgments

This work was financially supported by the Natural Science Foundation of China (Grant No. 21076204) and the Ministry of Science and Technology of China (Grant No. 2012CB215403). W.P. Sun also gratefully acknowledges the China Scholarship Council for partial financial support.

Appendix A. Supplementary material

Supplementary material associated with this article can be found, in the online version, at doi:10.1016/j.jpowsour.2012.05.065.

References

[1] B.C.H. Steele, A. Heinzel, Nature 414 (2001) 345–352.
[2] N.P. Brandon, S. Skinner, B.C.H. Steele, Annu. Rev. Mater. Res. 33 (2003) 183–213.
[3] Z.P. Shao, S.M. Haile, Nature 431 (2004) 170–173.
[4] T. Suzuki, Z. Hasan, Y. Funahashi, T. Yamaguchi, Y. Fujishiro, M. Awano, Science 325 (2009) 852–855.
[5] E.D. Wachsman, K.T. Lee, Science 334 (2011) 935–939.
[6] J.B. Goodenough, Annu. Rev. Mater. Res. 33 (2003) 91–128.
[7] K. Eguchi, T. Setoguchi, T. Inoue, H. Arai, Solid State Ionics 52 (1992) 165–172.
[8] R. Doshi, V.L. Richards, J.D. Carter, X.P. Wang, M. Krumpelt, J. Electrochem. Soc. 146 (1999) 1273–1278.
[9] B.C.H. Steele, Solid State Ionics 129 (2000) 95–110.
[10] A. Atkinson, Solid State Ionics 95 (1997) 249–258.
[11] T. Hashida, K. Sato, Y. Takeyama, T. Kawada, J. Mizusaki, ECS Trans. 25 (2009) 1565–1572.
[12] S.G. Kim, S.P. Yoon, S.W. Nam, S.H. Hyun, S.A. Hong, J. Power Sources 110 (2002) 222–228.
[13] Q.L. Liu, K.A. Khor, S.H. Chan, X.J. Chen, J. Power Sources 162 (2006) 1036–1042.
[14] S. Cho, Y.N. Kim, J.H. Kim, A. Manthiram, H.Y. Wang, Electrochim. Acta 56 (2011) 5472–5477.
[15] E.D. Wachsman, P. Jayaweera, N. Jiang, D.M. Lowe, B.G. Pound, J. Electrochem. Soc. 144 (1997) 233–236.
[16] E.D. Wachsman, Solid State Ionics 152–153 (2002) 657–662.
[17] J.Y. Park, H. Yoon, E.D. Wachsman, J. Am. Ceram. Soc. 88 (2005) 2402–2408.
[18] J.S. Ahn, D. Pergolesi, M.A. Camaratta, H. Yoon, B.W. Lee, K.T. Lee, D.W. Jung, E. Traversa, E.D. Wachsman, Electrochem. Commun. 11 (2009) 1504–1507.
[19] K.T. Lee, D.W. Jung, M.A. Camaratta, H.S. Yoon, J.S. Ahn, E.D. Wachsman, J. Power Sources 205 (2012) 122–128.
[20] D. Hirabayashi, A. Tomita, T. Hibino, M. Nagao, M. Sano, Electrochem. Solid-State Lett. 7 (10) (2004) A318–A320.
[21] A. Tomita, Y. Tachi, T. Hibino, Electrochem. Solid-State Lett. 11 (5) (2008) B68–B70.
[22] A. Tomita, S. Teranishi, M. Nagao, T. Hibino, M. Sano, J. Electrochem. Soc. 153 (6) (2006) A956–A960.
[23] W.P. Sun, L.T. Yan, B. Lin, S.Q. Zhang, W. Liu, J. Power Sources 195 (10) (2010) 3155–3158.
[24] W.P. Sun, L.T. Yan, Z. Shi, Z.W. Zhu, W. Liu, J. Power Sources 195 (15) (2010) 4727–4730.
[25] G.Y. Meng, C.R. Jiang, J.J. Ma, Q.L. Ma, X.Q. Liu, J. Power Sources 173 (2007) 189–193.
[26] X.G. Zhang, M. Robertson, C. Deces-Petit, W. Qu, O. Kesler, R. Maric, D. Ghosh, J. Power Sources 164 (2007) 668–677.
[27] M.F. Liu, R.R. Peng, D.H. Dong, J.F. Gao, X.Q. Liu, G.Y. Meng, J. Power Sources 185 (2008) 188–192.
[28] Y.H. Yin, W. Zhu, C.R. Xia, G.Y. Meng, J. Power Sources 132 (2004) 36–41.
[29] S.W. Zha, A. Moore, H. Abernathy, M.L. Liu, J. Electrochem. Soc. 151 (8) (2004) A1128–A1133.
[30] K.L. Duncan, K.-T. Lee, E.D. Wachsman, J. Power Sources 196 (2011) 2445–2451.
[31] W.P. Sun, Y.Z. Jiang, Y.F. Wang, S.M. Fang, Z.W. Zhu, W. Liu, J. Power Sources 196 (1) (2011) 62–68.
[32] A. Venkatasubramanian, P. Gopalan, T.R.S. Prasanna, Int. J. Hydrogen Energy 35 (10) (2010) 4597–4605.
[33] K.D. Kreuer, Annu. Rev. Mater. Res. 33 (2003) 333–359.
[34] E. Fabbri, D. Pergolesi, E. Traversa, Chem. Soc. Rev. 39 (2010) 4355–4369.
[35] L. Yang, S.Z. Wang, K. Blinn, M.F. Liu, Z. Liu, Z. Cheng, M.L. Liu, Science 326 (2009) 126–129.
[36] L. Yang, C.D. Zuo, S.Z. Wang, Z. Cheng, M.L. Liu, Adv. Mater. 20 (17) (2008) 3280–3283.
[37] L. Yang, Z. Liu, S.Z. Wang, Y.M. Choi, C.D. Zuo, M.L. Liu, J. Power Sources 195 (2010) 471–474.
[38] W.P. Sun, Z.W. Zhu, Y.Z. Jiang, Z. Shi, L.T. Yan, W. Liu, Int. J. Hydrogen Energy 36 (2011) 9956–9966.
[39] Y. Lee, J.H. Joo, G.M. Choi, Solid State Ionics 181 (2010) 1702–1706.
[40] B.D. White, O. Kesler, J. Power Sources 177 (2008) 104–110.